Journal of Magnetic Resonance **152,** 1–6 (2001)
doi:10.1006/jmre.2001.2351, available online at http://www.idealibrary.com on IDEAL®

Measurement of Interfluorine Distances in Solids

M. Lane Gilchrist, Jr.,[1] Kenji Monde,[2] York Tomita,[3] Takashi Iwashita,[4] Koji Nakanishi, and Ann E. McDermott[5]

Department of Chemistry, Columbia University, New York, New York 10027

Received September 18, 2000; revised February 28, 2001

^{19}F homonuclear dipolar recoupling methods were used to measure internuclear distances ranging from 5 to 12 Å in fluorinated organic compounds in the solid state. Magic-angle-spinning-based high-resolution techniques were utilized. Trifluoromethyl and aromatic fluorine groups were seperated by rigid aromatic spacers; these compounds were diluted into nonfluorinated host molecule matrices to give isolated homonuclear spin pairs with known internuclear distances. Radiofrequency-driven recoupling (RFDR) was used to elicit magnetization exchange between the spin pairs in 1D and 2D experiments. Simulation of the exchange was accomplished using a Monte Carlo-type algorithm to search the parameter space. These methods allow the determination of distances with an accuracy of 1 Å at shorter distances and 2 Å at longer distances, with the assumption of no prior knowledge of T_2^{ZQ}.

Key Words: **^{19}F NMR; solid state NMR; dipolar recoupling; MAS.**

We describe ^{19}F homonuclear distance measurements in the range 5–12 Å using fluorinated model compounds with rigid aromatic intrafluorine spacers. Solid state NMR (SSNMR) methods for measuring internuclear distances have been developed and used to characterize complex heterogeneous solids (*1*). ^{13}C–^{13}C distances of up to 7 Å have been measured (*2*). Since the gyromagnetic ratio of ^{19}F is 3.7 times greater than that of ^{13}C, the stronger dipolar couplings will allow measurements of longer distances as given by the relation $\nu_D = (\mu_0/4\pi)\hbar\gamma_1\gamma_2/4\pi^2 r_{IS}^3$; this fact has been exploited in studies of ^{19}F heteronuclear couplings in proteins by Schaefer and co-workers (*3, 4*) and studies of ^{19}F homonuclear couplings by Drobny, Stringer and, coworkers (J. Stringer, Ph.D. thesis, 1999). We report here that distances of up to 12 Å can also be conveniently measured with homonuclear ^{19}F methods.

This study serves to calibrate and validate distance limits for fluorine, and is the first step toward measuring ^{19}F–^{19}F internuclear distances in biological systems. The distance marker compounds for ^{19}F–^{19}F homonuclear distance measurements were designed with several considerations in mind: (1) the fluorine shifts for the two sites are resolved from one another; (2) the ^{19}F-labeled sites are rigidly separated in a solid state structure so that the distance is rigorously known; (3) the spin–lattice relaxation times (T_1) for all sites are short; and (4) the fluorine-bearing molecules were diluted into a nonfluorinated host to prevent intermolecular magnetic interactions. The trifluoromethyl group has some advantages relative to an aliphatic or aromatic fluorine group, such as enhanced detection sensitivity, facile proton decoupling, and favorable spin–lattice relaxation rates. Fluorines in trifluoromethyl groups used in this study typically had relaxation times ranging from 0.5 to 3.5 s as measured with an inversion recovery sequence, while many aromatic fluorines exhibited relaxation times of 20 s or longer. Chemical shift dispersion in one case resulted from a thioether linkage for one trifluoromethyl while the other group was directly attached to the aromatic carbon; the spectral separations were 20 ppm. In another case an adjacent β N group caused a upfield shift of ~8 ppm for one trifluoromethyl group relative to the other. In proteins, good dispersion might result simply from packing effects. The ^{19}F nucleus exhibits good dispersion of isotropic chemical shifts in fluorinated proteins, owning to the strong effects of van der Waals and electrostatic interactions on the ^{19}F shifts (*5*). At ambient temperatures, the rotation of the trifluoromethyl group is fast on the NMR chemical exchange time scale, giving rise to a single resonance with three times the intensity of a monofluoro label. The motionally averaged chemical shift anisotropy ($\Delta\delta \sim 30$ ppm) results in a spectrum consisting of a single centerband with modest magic angle spinning (MAS) rates while the anisotropy of the aromatic fluorine group ($\Delta\delta \sim 100$ ppm) results in substantial sideband intensities unless ultrafast spinning speeds are used. As a useful approximation such AX_3 spin systems can be treated as a single-spin system when the motion is in the fast limit. Distances between the sites were calculated from energy-relaxed structures using Macromodel 5.0 (with $\varepsilon = 3$). The effective distance between trifluoromethyl spin systems was computed from the average of $1/r^3$ for all pairs of spins, using

[1] Current address: Chemical Engineering Department, City College of New York, New York, NY 10031.

[2] Current address: Institute for Chemical Reaction Science, Tohoku University, 2-1-1 Katahira, Sendai 980-77, Japan.

[3] Current address: NIH/NIDR 30/223, Bethesda, MD 20892.

[4] Current address: Suntory Institute for Bioorganic Research, 1-1-1 Shimamoto-cho, Mishima-gun, Osaka 618, Japan.

[5] To whom correspondence should be addressed.

1090-7807/01 $35.00

the relation

$$\mathbf{r}_{\text{eff}} = \left(\sum_{i,j} (1/\sqrt[3]{\mathbf{r}_{ij}})/N \right)^{-1/3},$$

where N is the number of pairs of spins.

The expected gain in detection sensitivity for ^{19}F direct excitation MAS NMR experiments as compared with ^{13}C cross polarization MAS experiments is partially offset by hardware-specific losses (approx. 2 dB) due to the need for isolation of the proton transmitter from the ^{19}F receiver (>100 dB). Compounding this is the fact that in many cases fluorine linewidths are in excess of 1 ppm full width at half-maximum (FWHM). Commonly these linewidths are dominated by inhomogeneous broadening due to the much greater sensitivity of the chemical shift of fluorine to the local environment. This statement is based on our ability to perform hole-burning excitation within the MAS linewidth, and on comparison of T_2 values with linewidths. Room temperature spin–spin relaxation times (T_2) were measured with spin–echo methods and ranged from 0.8 to 5 ms, corresponding to intrinsic linewidths in the range 0.08–0.4 kHz. These values did not appear to exhibit systematic differences for aromatic fluorine vs trifluoromethyl sites. With the exception of the most structurally homogeneous samples (prepared by sublimation), the ^{19}F spectra generally exhibited additional linewidth contributions above the homogeneous estimate, FWHM $= 1/\pi T_2$. Typically, the linewidth was not limited by proton decoupling efficiency. For deuterated samples such as perdeuterated and diluted BTFQ, the T_2 values were only slightly longer than for the protonated cases (HBTFQ, 0.71 and 0.68 ms; dBTFQ, 1.05 and 1.17 ms). In practice, the detection sensitivity for a single trifluoromethyl group was typically twofold greater than for a single ^{13}C, but an aromatic fluorine was no better. We have been able to detect as few as 10 nanomoles of trifluoromethyl-containing molecules after a few hours of signal averaging. Other workers have utilized methods based on indirect detection of fluorine. In the experiments initiated by Schaefer and co-workers (*3*, *4*), the higher gyromagnetic ratio of fluorine was exploited for the enhanced dipolar strength while detection is carried out on a nucleus with a narrower linewidth and comparable or better sensitivity, such as ^{13}C or ^{31}P.

Preparation of the compounds was accomplished as follows (see Scheme 1). Bis(2,8-trifluoromethyl)-4-quinolinol (**1**, BTFQ), 4-hydroxyquinoline (**2**, 4HQ), and 7-(trifluoromethyl)-4-quinolinol were purchased from Aldrich. 6-Fluoro-4-hydroxy-2-(trifluoromethyl)quinoline (**3**, FTFQ) was obtained from Oakwood Products. Perdeuteration of **1** (BTFQ) and **2** was achieved via an alkaline-catalyzed deuterium–hydrogen exchange reaction in a microwave oven (*6*). Sequential microwave irradiation resulted in 83% deuteration for the fluorinated compound and 98% deuteration for the dilutant. The biphenyl fluorinated compound **5a** was synthesized using the Suzuki coupling (*7*–*9*). Bromothioanisole **3a** was cross-coupled to

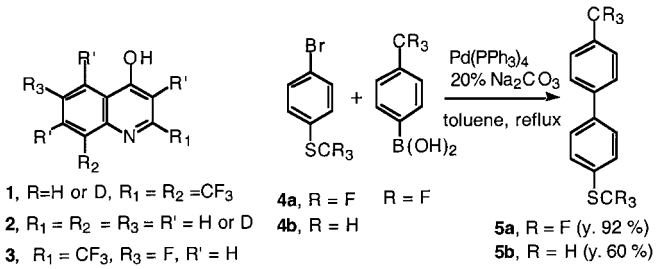

SCHEME 1

4-trifluoromethylbenzeneboronic acid under a $Pd(PPh_3)_4$ catalyst to give the biphenyl compound **5a** in 92% yield. In order to avoid intermolecular dipolar couplings from neighboring fluorine compounds, the fluorinated compounds were diluted by cocrystallization with structurally similar nonfluorinated analogues, which were prepared in a similar manner (e.g., **2**, **5b**). The crystalline samples were analyzed by HPLC to determine the ratio of fluorinated guest to nonfluorinated host. The most reliable method for obtaining good sample homogeneity was by rapid cooling of saturated solutions to form microcrystals. Samples with significant inhomogeniety or inadequate dilution were recognized by spurious intermolecular magnetization exchange contributions. Significant intermolecular exchange gives rise to biphasic curves. In these cases we were unable to simulate the data using the known internuclear separation. Furthermore, for some of the molecules used, samples made with the same fluorinated compound but with dilutions below that reported gave essentially identical exchange curves.

Figure 1 shows the pulse sequences used in these studies. For the 1D inversion exchange RFDR experiment (top), a DANTE (*d*elays *a*lternating with *nut*ation for selective *e*xcitation) sequence (*10*) was used to prepare an initial $\langle \mathbf{I}_z - \mathbf{S}_z \rangle$ polarization. This was followed with a radiofrequency-driven recoupling (RFDR) mixing sequence during the variable mixing time (*11*). Remaining longitudinal magnetization was subsequently detected with a readout pulse. High-power proton decoupling was employed in each sequence, with proton B_1 fields of 100 kHz. We have suppressed losses from ^{19}F–^{1}H Hartman–Hahn matching during the ^{19}F pulses by phase switching the decoupling at the midpoint of the mixing period π pulses. These points were extracted from 1D spectra collected at each mixing time. The magnetization exchange curves (Fig. 2) consist of normalized difference magnetization, $\langle \mathbf{I}_z - \mathbf{S}_z \rangle(t)/\langle \mathbf{I}_z - \mathbf{S}_z \rangle(0) \cdot k(t)$, plotted as a function of mixing time. Magnetization exchange is evidenced as a decrease in $\langle \mathbf{I}_z - \mathbf{S}_z \rangle$ as a function of mixing time. Normalization was performed by dividing the difference intensity value for each mixing time, $\langle \mathbf{I}_z - \mathbf{S}_z \rangle(t)$, by the corresponding zero-time value, $\langle \mathbf{I}_z - \mathbf{S}_z \rangle(0)$, followed by a multiplicative correction for relaxation processes and other losses, $k(t)$. This correction, $k(t)$, was based on two control experiments: analogous data were collected for a singly trifluoromethyl-labeled sample (with similar T_2 and T_1 values); in addition, we measured

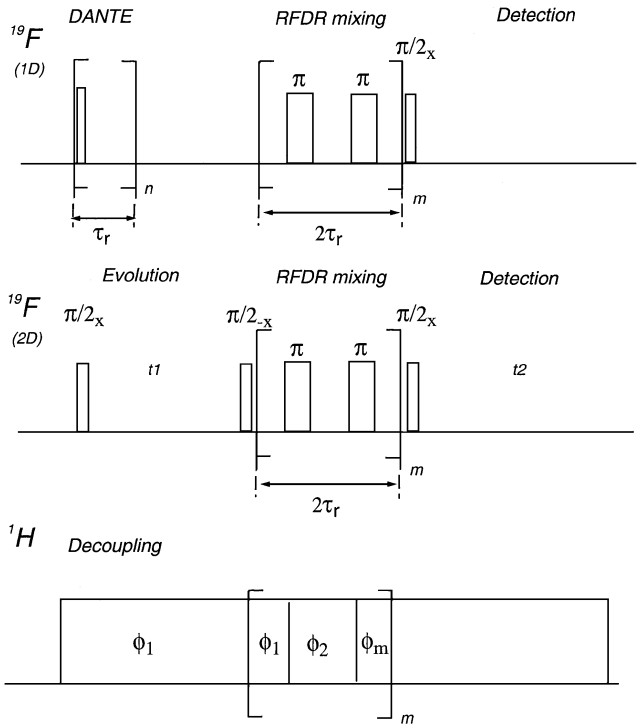

FIG. 1. One- and two-dimensional RFDR pulse sequences used in fluorine distance measurements. In the 1D sequence (top), the DANTE sequence was used to prepare the $\langle \mathbf{I}_z - \mathbf{S}_z \rangle$ initial polarization before the variable RFDR mixing period, which is composed of rotor synchronized π pulses. For the 2D experiments (middle sequence), the variable t_1 evolution period was followed by a nonselective $\pi/2$ pulse to create longitudinal magnetization prior to the RFDR mixing. In both versions a $\pi/2$ readout pulse was applied prior to the detection of the FID. To suppress losses of ^{19}F magnetization the proton decoupling was phase switched at the midpoint of the pulse sequence π pulses (bottom).

signal losses incurred by applying a π pulse train in a fashion identical to the RFDR sequence but without the DANTE inversion. If integrated peak areas were used instead of intensities, similar curves resulted. Figure 2 shows several RFDR 1D inversion exchange data sets along with simulations (solid curves) and corresponding molecular structures.

Two other versions of the RFDR experiment had the advantage of internal correction for systematic signal intensity losses: 2D magnetization exchange RFDR (*11*, *12*) and 1D saturation exchange RFDR. In the 2D magnetization exchange RFDR experiment, shown in the middle sequence in Fig. 1, the **I** and **S** spins are initially frequency labeled during a variable evolution time in the transverse plane. At the end of the t_1 evolution the longitudinal magnetization is restored and the RFDR mixing sequence is applied over the specified mixing time. A readout pulse is applied prior to the collection of the FID for each t_1 slice. In the 2D experiments, the build-up curve is recorded: the cross-peak volume is normalized relative to total peak volume from the 2D spectra taken for each mixing time. For the case of the 1D saturation exchange RFDR experiment the same pulse sequence is used as for the inversion exchange. We present in Fig. 3 the ratio of the magnetization exchange (the cross-peak intensity in the 2D, or increase in $\mathbf{S}_z$ in the saturation exchange) to the total intensity, $\langle \mathbf{S}_z \rangle / \langle \mathbf{I}_z + \mathbf{S}_z \rangle$, for the same compounds as displayed in Fig. 2. From all of these data sets it is evident that the rate of magnetization exchange slows dramatically as the intermolecular separation is increased. The 2D or saturation transfer experiments appear to be a more reliable way to measure the exchange curves, since the correction for losses is substantial. On the other hand, it is worth noting that the detection sensitivity for the 2D exchange or saturation recovery experiment is significantly worse than the 1D inversion exchange experiment.

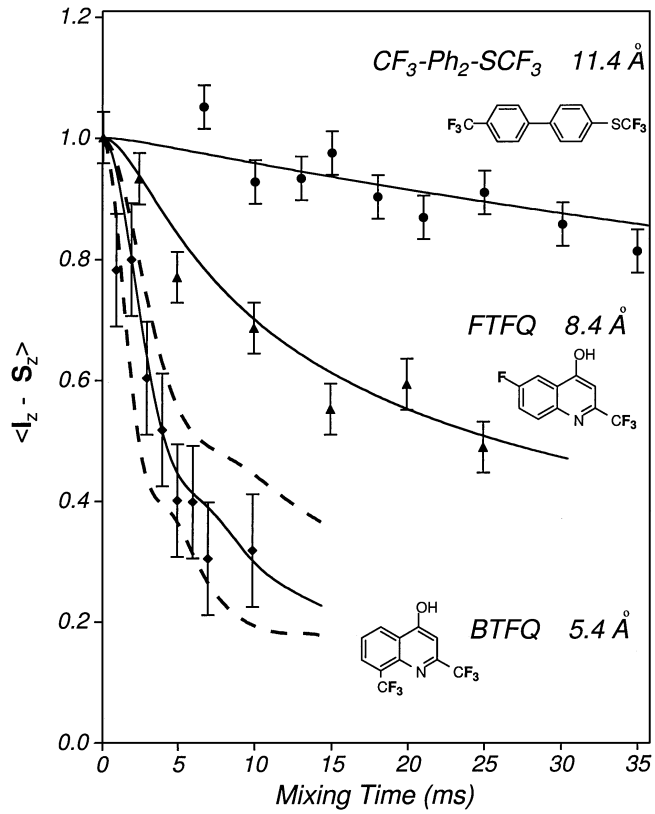

FIG. 2. RFDR magnetization exchange data and simulated exchange curves (solid lines) corresponding to each compound; the computed fluorinated spin system separations are indicated. The dilutions for 2,8-bis(trifluoromethyl)-4-quinolinol (BTFQ) **(1)**, 6-Fluoro-4-hydroxy-2-(trifluoromethyl) quinoline (FTFQ) **(3)**, 4-(trifluoromethyl)-4′-(trifluoromethylthio) biphenyl (CF_3–Ph_2–SCF_3) **(5a)** were 0.29, 0.25, and 0.23 mole%, respectively. Absolute numbers of spins were in the range of 0.01–2 μmoles, and individual exchange curve points were obtained by averaging for up to 6 h. In the data from 4-(trifluoromethyl)-4′-(trifluoromethylthio)biphenyl **(5a)**, an unwanted fast component from 0–5 ms was removed, presumably arising from a minor fraction of the sites in which intermolecular magnetization exchange occurred. The dashed curves at the bottom are examples of simulations at the boundaries of acceptable agreement with experiment, with RMSD values of 0.12, which is $2 \cdot \mathrm{RMSD}_{\min}$ (0.06). These curves were simulated using fixed T_2^{ZQ} values (3.1 ms) at internuclear separations (r_{IS}) of 5.1 and 6.4 Å for the bottom and top dashed curves, respectively. The spinning speeds were 12.9 kHz for BTFQ and FTFQ and 12 kHz for CF_3–Ph_2–SCF_3. Larmor frequency was 373.013 MHz; the experiments were carried out at room temperature.

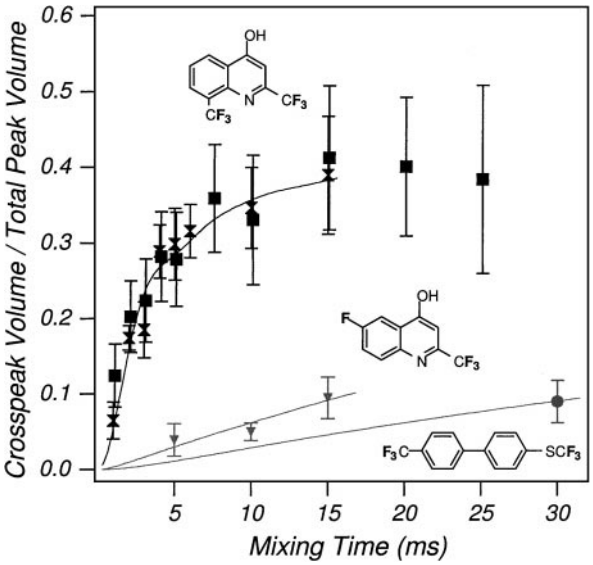

FIG. 3. Two-dimensional RFDR magnetization exchange data and simulated exchange curves (solid lines) corresponding to each compound; the computed fluorinated spin system separations are indicated. The square data points are from a saturation exchange experiment performed on BTFQ. The spinning speeds were 12.9 kHz for BTFQ and 12 kHz for FTFQ and CF_3–Ph_2–SCF_3. Larmor frequency was 373.013 MHz; the experiments were carried out at room temperature.

The 2D approach will have obvious virtue when multiple sites are labeled.

As previously described in a theoretical treatment of the effect of the RFDR mixing sequence (*11*), the mixing curves should depend on the chemical shift difference between the two sites, the MAS speed, various relaxation processes, and the intersite distance, r_{IS}. Simulations (*12*) of these curves are shown as solid lines. The simulated curves are derived from calculations of $\langle \mathbf{I}_z - \mathbf{S}_z \rangle$ for the 1D inversion exchange case and $\langle \mathbf{S}_z \rangle / \langle \mathbf{I}_z + \mathbf{S}_z \rangle$ for the 2D RFDR case, both computed as a function of mixing time. Parameters used in the calculations are listed in Table 1. Some parameters were measured with supplemental experiments. Principal values of the CSA tensors were obtained from computer simulations of the spinning sideband intensities of MAS spectra (*13*) and agree well with previous values for similar compounds (*14–16*). Relative CSA tensor orientations were estimated based on the molecular structure and previous literature analysis of the CSA axes. Trifluoromethyl groups were assumed to have axially symmetric CSA tensors with the *z* axis of the principal axis system directed along the C–C bond (*14*). For the aromatic fluorine group, the CSA principal axis was normal to the plane of the aromatic ring, as determined in earlier studies (*15, 16*). Euler angles describing the CSA principal axis system relative to the dipolar axis system (Table 1) were calculated based on the minimum energy structures. Thus the only unknown simulation parameter is the zero-quantum coherence relaxation time, T_2^{ZQ}. This quantity has previously been estimated by the relation $1/T_2^{ZQ} = 1/T_2^{I} + 1/T_2^{S}$, corresponding to the assumption that the zero-quantum coherence decay is caused by uncorrelated fluctuating fields at each site (*17*).

In a typical structure problem, r_{IS}, T_2^{ZQ}, and the Euler angles are unknown. In order to extract r_{IS} from an exchange curve without prior knowledge of the CSA, Euler angles, or T_2^{ZQ}, we have constructed processing software based on a Monte Carlo-type

TABLE 1

Compound	r_{IS} (Å)[a]	Dipolar coupling (Hz)[b]	CSA site 1 (ppm)[c] $\sigma_{11}\sigma_{22}\sigma_{33}$	CSA site 2 (ppm)[c] $\sigma_{11}\sigma_{22}\sigma_{33}$	T_1 (s)[d] Site 1	T_1 (s)[d] Site 2	T_2 (ms)[e] **lw(kHz)**[f] Site 1	T_2 (ms)[e] **lw(kHz)**[f] Site 2	CSA PAS to dipolar PAS[g] Ω_{PD}^{I} α_1 β_1 γ_1	CSA PAS to dipolar PAS[g] Ω_{PD}^{S} α_2 β_2 γ_2
BTFQ (**1**)	5.4	676	−80.0	−89.0			0.71	0.68	0.0	0.0
			−80.0	−89.0	0.5	2.0			107.3	41.5
			−16.0	−21.0			**1.3**	**1.4**	0.0	0.0
FTFQ (**3**)	8.4	180	−88.6	−166.6			0.41	0.44	0.0	82.0
			−88.6	−127.0	2.6	3.3			10.0	90.0
			−38.4	−54.1			**1.2**	**1.8**	0.0	7.0
$CF_3Ph_2SCF_3$ (**5a**)	11.4	72	−59.8	−78.6			4.4	2.9	0.0	0.0
			−59.8	−78.6	0.5	0.7			8.4	122.7
			1.2	−18.6			**0.5**	**0.7**	0.0	0.0

[a] Calculated with MacroModel 3.0.
[b] Computed from r_{IS}.
[c] Calculated from MAS sideband patterns—axial symmetry was assumed for the trifluoromethyl group.
[d] Obtained from inversion recovery experiment.
[e] Obtained from spin echo experiment.
[f] Based on full-width half-maximum linewidth values from 1D spectra.
[g] Computed from molecular geometry.

algorithm (*18, 19*). Random or biased moves in the parameter space are followed by evaluation of the root mean square deviation (RMSD) between the simulated (*12*) and experimental magnetization exchange curves, where N is the number of points in the experimental curve:

$$\mathrm{RMSD} = 1/\sqrt{N-1}\left(\sum_{i=1}^{N}(\boldsymbol{x}_{i,\mathrm{sim}} - \boldsymbol{x}_{i,\mathrm{exp}})^2\right)^{1/2}.$$

Simulations were considered to have acceptable agreement with experiment when the RMSD was less than twice that of the best fit (~95% confidence interval). Root mean square deviations between a smooth spline polynomial fit and the data, or between global best fit and data, were typically comparable and were typically of order of 5% of the maximal intensity data point. These values were also comparable to RMSD expected from the inherent noise in the data, indicating that the RMSD values for the global best fit are dominated by inherent noise in the data rather than by systematic fitting errors as would be expected if the sample were not sufficiently dilute. In typical simulations there are two open fitting parameters: the internuclear distance and the zero-quantum dephasing time, T_2^{ZQ}. There are also five highly constrained fitting parameters: overall scaling, isotropic shifts of both sites, and CSA widths for both sites. Eight additional parameters are typically much less influential: the Euler angles, and the asymmetry of the CSA for each site. Reported uncertainty estimates in the distance measurements (r_{IS}) were based on the results of the exploration of T_2^{ZQ} values ranging from 0.5 to 6 ms. In Fig. 4, the top 3D plot displays the RMSD values from an unconstrained parameter space search as a function of T_2^{ZQ} and r_{IS}. The middle plot shows the 2D projection onto the xy plane of simulations below the RMSD cutoff value ($\mathrm{RMSD} \leq 2 \times \mathrm{RMSD}_{\mathrm{min.}}$), bounding the region of acceptable simulations to be used in the determination of the uncertainty in the internuclear distance. As an example, two simulated curves at the maximum acceptable RMSD boundary are shown in the bottom of Fig. 2 as the dashed curves.

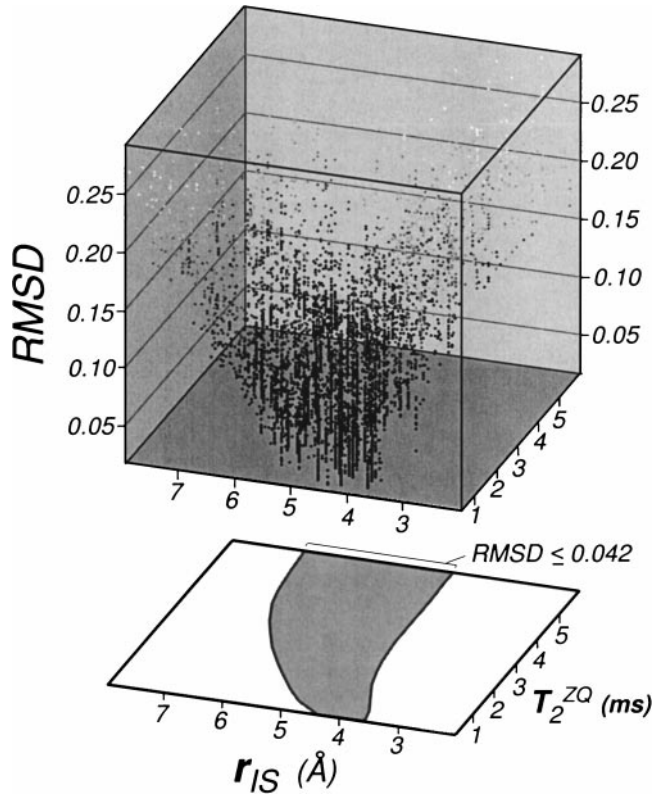

FIG. 4. Uncertainty in the interfluorine distance (r_{IS}) from 2D RFDR of BTFQ was derived by sampling the parameter space and comparing root-mean-square deviations between simulation and experimental data points for various parameter sets. The top panel shows the RMSD values obtained from 10,000 calculations along the z axis, while two important fitting parameters (zero-quantum dephasing time, T_2^{ZQ}, and interfluorine distance values r_{IS}) are the x and y axes. In this simulation, Euler angles and the CSA parameters were allowed to vary (range for $\Delta\sigma_{\mathrm{iso}} = 1$ ppm; Δanisotropy $= 20$ ppm; $\Delta\eta = 0.2$). The bottom panel displays the 2D projection of the subset of T_2^{ZQ} and interfluorine distance values (r_{IS}) for which simulation acceptable RMSD values were observed ($\mathrm{RMSD} \leq 2 \cdot \mathrm{RMSD}_{\mathrm{min.}}$).

Monte Carlo searches were performed subject to various assumptions about the parameter values; Table 2 describes the values for the internuclear distances for which simulations exhibit acceptable RMSD values. We allowed for a broad range of T_2^{ZQ} and r_{IS}, and we allowed for all possible values of $\Omega^{\mathrm{I}}_{\mathrm{PD}}(\alpha_1, \beta_1, \gamma_1)$ and $\Omega^{\mathrm{S}}_{\mathrm{PD}}(\alpha_2, \beta_2, \gamma_2)$, with the limits; $0^\circ \geq \alpha_1, \gamma_1, \alpha_2, \gamma_2 \geq 360^\circ$ and $0^\circ < \beta_1, \beta_2 < 180^\circ$. Furthermore the isotropic chemical shifts were allowed to vary over 1 ppm and the CSA width over 20 ppm, and the asymmetry parameter varied from 0.0 to 0.2. The results of such an unconstrained search of parameter space are shown in Fig. 4 (top). In other more constrained fits, all the chemical shift parameters were fixed and the polar Euler angles were only allowed to range over $\pm 10^\circ$ from the ideal values estimated from molecular geometry and based on previous studies (*14–16*). Finally, in a two-dimensional search, only T_2^{ZQ} and r_{IS} were allowed to vary. The data in Table 2 indicate that with the exception of the T_2^{ZQ}, knowledge of the other parameters is not important for the error bound for the distance determination: in other words whether these additional parameters were constrained did not have an important effect on our estimated error bounds. The cases under discussion are in the fast MAS limit where spinning sideband intensities are low: if instead the shielding tensors were overlapping and the spinning speed were relatively low, then these other fitting parameters would have been much more important. We have also determined the uncertainties for the 2D RFDR measurements in a similar fashion. Best fit and actual values of the internuclear distance are compared in Table 2. The precision and accuracy is within 1 Å for BTFQ and FTFQ, even in the worst case where $\Omega^{\mathrm{I}}_{\mathrm{PD}}(\alpha_1, \beta_1, \gamma_1)$, $\Omega^{\mathrm{S}}_{\mathrm{PD}}(\alpha_2, \beta_2, \gamma_2)$, T_2^{ZQ}, and r_{IS} are unknown. The results for the longest distance compound, $CF_3Ph_2SCF_3$, reflect the fact that we are nearing the maximum distance limit for the method but nevertheless the accuracy is within 2 Å in all cases.

TABLE 2

	$r_{(IS)}$ (Å)[a]			
	Fixed Ω^I_{PD}, Ω^S_{PD}	$0^\circ \geq \alpha_1, \gamma_1, \alpha_2, \gamma_2 \geq 360^\circ$ $\beta_1, \beta_2 \pm 10^\circ$	$0^\circ \geq \alpha_1, \beta_1, \gamma_1, \alpha_2, \beta_2 \gamma_2 \geq 360^\circ$	$r_{(IS)}$ (Å)[b] calculated
1D RFDR inversion exchange				
BTFQ (**1**)	5.8 ± 1.7	6.0 ± 2.5	5.9 ± 2.8	5.4
FTFQ (**3**)	7.6 ± 3.0	7.9 ± 3.0	7.5 ± 3.0	8.4
$CF_3Ph_2SCF_3$ (**5a**)	12.0 ± 3.0	13.2 ± 4.0	13.2 ± 4.0	11.4
2D RFDR exchange				
BTFQ (**1**)	5.5 ± 0.3	6.3 ± 1.7	4.9 ± 1.6	5.4
FTFQ (**3**)	8.6 ± 3.0	8.7 ± 2.8	8.9 ± 3.1	8.4
$CF_3Ph_2SCF_3$ (**5a**)	12.6 ± 3.5	11.9 ± 4.0	11.3 ± 4.0	11.4

[a] Based on global best fit (lowest RMSD), in a search with only r_{IS} and T_2^{ZQ} varied. $RMSD_{min.}$ was roughly 3–5% and was dominated by experimental signal-to-noise. Uncertainty was obtained from a range of distances in simulations with $RMSD \leq 2 \cdot RMSD_{min.}$, representing a ~95% confidence interval.
[b] From minimum energy structures computed by Macromodel 5.0.

It is important to note that if we can further constrain the simulation by incorporating an experimentally derived value of T_2^{ZQ}, the uncertainty in the distance measurement decreases significantly, *even for dilute samples with limited sensitivity and significant experimental error.* For the compound with the longest internuclear distance (CF_3–Ph_2–SCF_3; 11.4 Å), for 1D measurements the uncertainty could conceivably be reduced from roughly 3 to 1.2 Å for the fixed Euler angles case and from roughly 4 to from 2 Å for the unconstrained case, a greater than 50% reduction. For every sample in our survey the estimate based upon linewidths or on Carr–Purcell dephasing curves did not usefully constrain the fit. Rather, these estimates for T_2^{ZQ} were typically too short and gave artificially short distances. Preliminary experiments in which the dephasing time of the zero-quantum coherence was indirectly measured confirmed the suggestion that it is somewhat longer than that predicted by Carr–Purcell measurements. For samples with multiple fluorine labels, multispin relaxation dynamics might become a more important issue in the error analysis.

In summary, these data indicate that distances in the range of 5–12 Å can be measured with an accuracy of 1.0 Å at short range and 2.0 Å at long range without prior knowledge of T_2^{ZQ}. This accuracy will increase considerably if an experimental measurement of T_2^{ZQ} is obtained. Such an extension of the distance range from that of ^{13}C-based methods provides a means for measuring intermolecular and interdomain distances in biological systems. ^{19}F SSNMR of biological systems has several other attractive features; we envision many applications of this method in structural biology as well.

ACKNOWLEDGMENTS

The authors acknowledge support from the Kanagawa Academy of Science and Technology, and the NIH (GM61131 (A.E.M.), GM50291 (K.N.), and AI10187 (M.L.G.)).

REFERENCES

1. J. M. Griffiths and R. G. Griffin, Nuclear magnetic resonance methods for measuring dipolar couplings in rotating solids, *Anal. Chim. Acta* **283,** 1081–1101 (1993).
2. O. B. Peersen, S. Yoshimura, H. Hojo, S. Aimoto, and S. O. Smith, Rotational NMR measurements of internuclear distances in an a-helical peptide, *J. Am. Chem. Soc.* **114,** 4332–4335 (1992).
3. D. R. Studelska, C. A. Klug, D. D. Beusen, L. M. McDowell, and J. Schaefer, Long-range distance measurements of protein binding sites by rotational-echo double-resonance NMR, *J. Am. Chem. Soc.* **118,** 5476–5477 (1996).
4. L. M. McDowell, M. S. Lee, R. A. McKay, K. S. Anderson, and J. Schaefer, Intersubunit communication in tryptophan synthase by carbon-13 and fluorine-19 REDOR NMR, *Biochemistry* **35,** 3328–3334 (1996).
5. A. C. de Dios and E. Oldfield, Evaluating F-19 chemical shielding in fluorobenzenes—Implications for chemical-shifts in proteins, *J. Am. Chem. Soc.* **116,** 7453–7454 (1994).
6. G. J. Köves, Acid-catalysed deuterium exchange of aromatic protons. Part III: Accelerated exchange by microwave irradiation, *J. Lab. Comp. Radiopharm.* **34,** 255–262 (1994).
7. N. Miyaura, T. Yanagi, and A. Suzuki, The palladium-catalyzed cross-coupling reaction of phenylboronic acid with haloarenes in the presence of bases, *Synth. Com.* **11,** 513–519 (1981).
8. N. Miyaura, K. Yamada, H. Suginome, and A. Suzuki, Novel and convergent method for the stereo- and regiospecific synthesis of conjugated alkadiens and alkenynes via the palladium-catalyzed cross-coupling reaction of 1-alkenylboranes with bromoalkenes and bromoalkynes, *J. Am. Chem. Soc.* **107,** 972–980 (1985).
9. Y. Hoshino, N. Miyaura, and A. Suzuki, Novel synthesis of isoflavones by the palladium-catalyzed cross-coupling reaction of 3-bromochromones with arylboronic acid or its esters, *Bull. Chem. Soc. Jpn.* **61,** 3008–3010 (1988).
10. G. A. Morris and R. Freeman, Selective excitation in Fourier-transform nuclear magnetic resonance, *J. Magn. Reson.* **29,** 433–462, (1978).
11. A. E. Bennett, J. H. Ok, R. G. Griffin, and S. Vega, Chemical shift correlation spectroscopy in rotating solids: Radio frequency-driven dipolar recoupling and longitudinal exchange, *J. Chem. Phys.* **96,** 8624–8627 (1992).
12. A. E. Bennett, C. M. Rienstra, J. M. Griffiths, W. Zhen, P. T. Lansbury, and R. G. Griffin, Homonuclear radio frequency-driven recoupling in rotating solids, *J. Chem. Phys.* **108,** 9463–9479 (1998).
13. J. Herzfeld and E. Berger, Sideband intensities in NMR spectra of samples spinning at the magic angle, *J. Chem. Phys.* **73,** 6021–6030 (1980).
14. R. G. Griffin, J. D. J. Ellett, M. Mehring, J. G. Bullitt, and J. S. Waugh, Single crystal study of the 19-F shielding tensors of a trifluoromethyl group, *J. Chem. Phys.* **57,** 2147–2155 (1972).
15. M. Mehring, R. G. Griffin, and J. S. Waugh, 19F shielding tensors from a coherently narrowed NMR powder spectra, *J. Chem. Phys.* **55,** 746–757 (1971).
16. H. Raber and M. Mehring, F19 chemical shift tensor in fluorobenzene compounds, *Chem. Phys.* **26,** 123–130 (1977).
17. A. Kubo and C. A. McDowell, Spectral spin diffusion in polycrystalline solids under magic-angle spinning, *J. Chem. Soc. Faraday Trans.* **84,** 3713–3730 (1988).
18. N. Metropolis, A. W. Rosenbluth, M. N. Rosenbluth, A. H. Teller, and E. Teller, *J. Chem. Phys.* **21,** 1087 (1953).
19. J. D. Trudeau, J. Bohmann, and T. C. Farrar, Parameter Estimation for longitudinal relaxation studies in coupled two-spin 1/2 systems using Monte Carlo simulations, *J. Magn. Reson.* **104,** 151–166 (1993).